ACCEPTED MANUSCRIPT

# Domain matched epitaxial growth of $Bi_{1.5}Zn_1Nb_{1.5}O_7$ thin films by pulsed laser deposition

P S Krishnaprasad[1], Aldrin Antony[2,3], Fredy Rojas[2], Joan Bertomeu[2], M K Jayaraj[1]

[1]*Cochin University of Science and Technology, Kochi-22, Kerala, India.*

[2]*Departament of Applied Physics and Optics, University of Barcelona, Spain.*

[3]*Department of Energy Science and Engineering, IIT Bombay, India.*

**Corresponding author**

*E-mail: mkj@cusat.ac.in, phone: +91484-2577404

**Abstract**

$Bi_{1.5}Zn_1Nb_{1.5}O_7$ (BZN) epitaxial thin films were grown by pulsed laser deposition on $Al_2O_3$ with a double ZnO buffer layer through domain matching epitaxy (DME) mechanism. The pole figure analysis and reciprocal space mapping revealed the single crystalline nature of the thin film. The pole figure analysis also shows a $60^0$ twinning for the (222) oriented crystals. Sharp intense spots in the SAED pattern also indicate the high crystalline nature of BZN thin film. The Fourier filtered HRTEM images of the BZN-ZnO interface confirms the domain matched epitaxy of BZN with ZnO buffer. An electric field dependent dielectric tunability of 68% was obtained for the BZN thin films with inter digital capacitors patterned over the film.

**Keywords:** Domain matching epitaxy; pulsed laser deposition; Bismuth Zinc Niobate; HRTEM.

ACCEPTED MANUSCRIPT

## 1. Introduction

Dielectric–semiconductor heterostructures are of great interest for electronic and optoelectronic applications ranging from communication devices to satellite services [1-4]. Each application imposes different requirements for the dielectric materials, among which the most desired properties are large tunability combined with a low microwave loss. The polycrystalline dielectric thin films often show lower permittivity as compared to the bulk whereas high quality epitaxial films can have a permittivity close to that of single crystal [1,5,6]. Interfacing dielectric oxides with semiconductors will allow us to take advantage of such material properties for multi-functional devices. While growing dielectric thin films, the oxidation at the film-substrate interface can degrade the electrical properties of the heterostructure, which demand the use of buffer layers [7] a necessity. An oxide semiconductor as the buffer layer eliminates this problem, thus offering a chemically stable heterostructure. Zinc oxide [8-9], indium oxide [10], and tin oxide [11] have been investigated for this purpose previously. Among these, ZnO is a promising wide band gap semiconductor and it has been widely used as buffer layer for the growth of dielectric films for different applications [12, 13]. Thus epitaxial growth and control of defects in thin films are very important requisites in the preparation of thin film heterostructures, as single defect may deteriorate the device performance.

Domain matching epitaxy (DME) deals with the matching of lattice planes, which could be different in different directions of the film–buffer interface. The misfit across the film-buffer interface is accommodated by matching of integral multiples of lattice planes of the film with those of buffer layer. The misfit can range from being very small to very large. In the small misfit regime, the DME reduces to lattice matching epitaxy (LME) where matching of the same planes or lattice constants is considered with a mismatch less than 7%–8%. If the misfit falls in between the perfect matching ratios of planes, then the size of the domain can vary in a

ACCEPTED MANUSCRIPT

ACCEPTED MANUSCRIPT

systematic way to accommodate the additional misfit. In DME, the initial misfit strain could be very large, but this can be relaxed by matching of integral multiples of the planes of the film across the film-buffer interface [14]. Bismuth zinc niobate (BZN) in its pyrochlore phase ($Bi_{1.5}Zn_1Ni_{1.5}O_7$) has been demonstrated as a potential candidate for microwave application due to its low dielectric loss and medium permittivity (ε) in the microwave region and compositionally tunable temperature coefficients of capacitance ($t_c$) [15]. Various single crystalline substrates, MgO, $SrTiO_3$, $Al_2O_3$, etc. are usually used for growing ferroelectric thin films [16-19]. Among these, $Al_2O_3$ possess advantages such as low cost, high chemical stability and a low loss tangent, and hence it is an excellent substrate for passive microwave components. Large lattice mismatch and different crystal structures of BZN and $Al_2O_3$ is the main hurdle for this heterostructure growth. Here we report the epitaxial growth of bismuth zinc niobate (BZN) thin films by buffer assisted domain matching epitaxy. The preliminary results of this work has been published elsewhere [20]. The present work confirms the domain matched epitaxial growth of BZN, where integral multiples of lattice spacing of BZN thin film and ZnO buffer layer match across film-buffer interfaces. The DME growth has been further confirmed using extensive calculations on matching planes across the film-buffer interface and Fourier filtered TEM images. Based on the Pole figure analysis, twinning of BZN crystals are also identified and discussed. The fabricated inter digital capacitors on BZN thin film possess large dielectric tunability with appreciably low dissipation factor.

## 2. Experiment

Various methods have been adopted for the deposition of oxide thin films. However for the deposition of oxide multinaries, laser assisted deposition and sputtering are ideal because only these techniques reproduce the composition of the starting target material in the film. In the

ACCEPTED MANUSCRIPT

present work, fourth harmonics of Q-switched Nd: YAG laser (266 nm) was used for ablation. The ablation was carried out at a laser fluence of 1.6 J/cm$^2$. The ceramic targets of $Bi_{1.5}Zn_1Nb_{1.5}O_7$ were prepared by the conventional solid-state ceramic synthesis route. High-purity (99.9%) $Bi_2O_3$, ZnO and $Nb_2O_5$ were used as the starting materials. The BZN powder was pressed into cylindrical disks of about 10 mm diameter and 5 mm thickness, by applying a pressure of 100 MPa. These cylindrical compacts, sintered at a temperature of 825 °C for 2 h, were used as the targets for PLD. Highly oriented BZN thin films were grown on (0001) oriented $Al_2O_3$ using a double layer ZnO buffer method. To achieve a high crystalline quality ZnO buffer layer which also has domain matching with BZN layer, a single ZnO buffer layer of ~ 20nm thickness was first deposited on $Al_2O_3$ at a substrate temperature of 300 ºC followed by a second ZnO layer of 20nm thickness deposited at a higher substrate temperature of 600 ºC. Both layers were grown at an oxygen partial pressure of $5\times10^{-4}$ mbar. BZN thin films were deposited on the ZnO buffer layer at a substrate temperature of 700 ºC in an oxygen partial pressure of 0.1 mbar. Each layer deposition was followed by a post deposition annealing at 700 ºC at an elevated oxygen partial pressure of about 0.5 mbar for a duration of 1hr.

High resolution X-ray diffraction (XRD) $\omega$-2$\theta$, pole figure and RSM measurements were performed on a PANalytical X'pert PRO diffractometer using monochromatic CuK$\alpha$ radiation ($\lambda$ = 1.54060 Å). The composition of the of the films was analyzed by energy-dispersive X-ray spectroscopy (EDS), using a JEOL JSM 6390 scanning electron microscope. The microstructural properties of the films were studied a using high-resolution transmission electron microscope JEOL-JEM-2100F. Specimens for the cross sectional TEM were prepared carefully by forming a sandwich of two pieces of the films, with the film sides facing each other using an epoxy followed by the mechanical polishing and argon ion milling using a Gatan 691 Precision Ion

ACCEPTED MANUSCRIPT

Polishing System (PIPS). Digital Micrograph software was used to analyze the selected area electron diffraction patterns and the high resolution images of the samples. A Gaussian mask with standard deviation equal to 5 pixels was applied in Fourier space. The nominal growth rate for BZN thin film was 0.055 nm $s^{-1}$ calibrated using the thickness measured from high resolution transmission microscopy (HRTEM) analysis.

### 3. Results and discussion

High resolution X-ray diffraction (HRXRD) was employed to determine the structural properties of thin films. The ω-2θ scan of BZN thin films grown on $Al_2O_3$ with and without ZnO buffer is shown in figure 1. It should be noted that the XRD scan in the figure 1 is shown in a logarithmic scale to illustrate the relative intensities and to reveal any potentially weak diffraction peaks. The ω-2θ scan for the BZN film deposited without buffer layer on to the $Al_2O_3$ substrate (figure 1b) shows the peak of BZN (222) at $29.07^0$, (004) peak at $33.5^0$ along with (444) at $60.11^0$. BZN thin film deposited with single ZnO buffer layer shows peaks of BZN as mentioned above together with reflection from ZnO (002) at $34.4^0$. Thus the BZN film directly grown on $Al_2O_3$ and with single ZnO buffer layer (figure 1b and 1c respectively) shows polycrystalline nature. On the other hand the BZN film on $Al_2O_3$ substrate with double ZnO buffer layer shows only the very strong (222) peaks of BZN without any reflections from other planes. The absence of other reflections implies a well aligned BZN (222) planes over the ZnO layer. The full width at half maximum of the BZN (222) peak is around $0.34^0$. The d-spacing of the BZN calculated from the XRD pattern is found to be 3.07 Å and it agrees close to that of bulk value (3.05Å). The composition analysis (EDS) on the thin films showed no significant variation of stoichiometry from that of the target except for a small decrease in $Zn^{2+}$ content, which might be due to the highly volatile nature of $Zn^{2+}$.

ACCEPTED MANUSCRIPT

ACCEPTED MANUSCRIPT

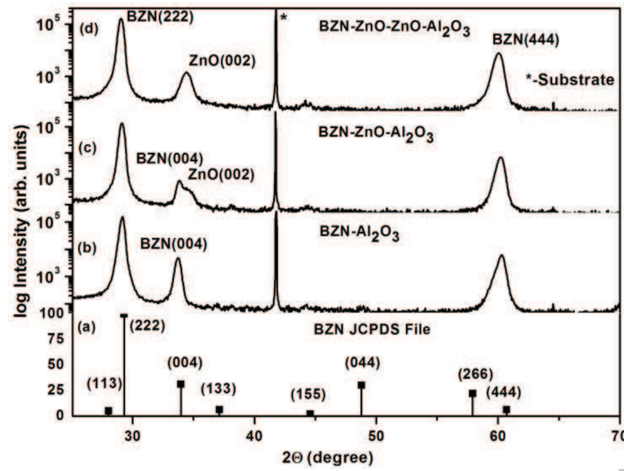


**Figure 1.** a) The JCPDS data of BZN and the XRD ω-2θ scan of the BZN film deposited b) directly on to $Al_2O_3$ substrate c) with single ZnO buffer layer and d) with double ZnO buffer layer.

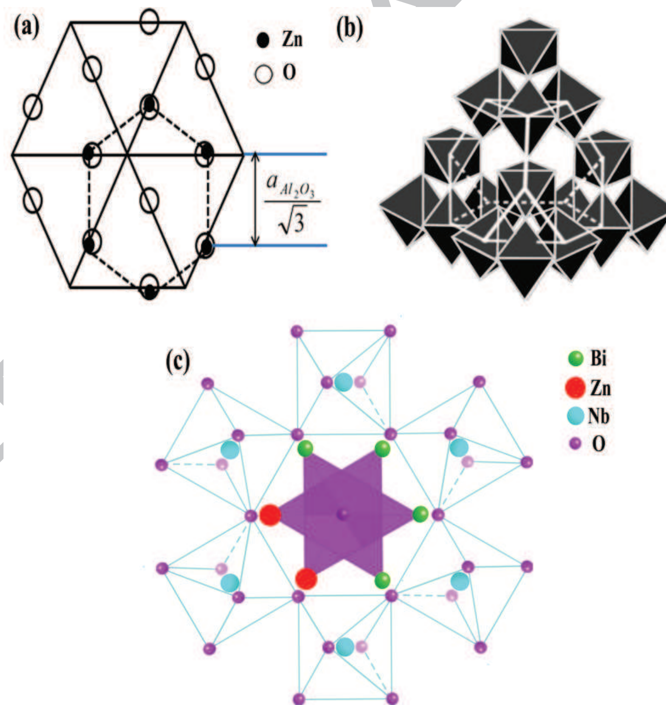


**Figure 2.** a) Schematic of arrangement of atoms in the basal plane of ZnO and $Al_2O_3$ b) $B_2O_6$ networks in the $A_2B_2O_7$ pyrochlore forming a hexagonal tungsten bronze structure c) The

ACCEPTED MANUSCRIPT

essentially hexagonal prismatic environment of the A cations in the $A_2B_2O_7$ pyrochlore structure type of BZN projected along [111].

Schematic representation of the Zn atoms in ZnO oriented over $Al_2O_3$ substrate is shown in the figure 2a. ZnO has hexagonal structure with a=3.24Å and c=5.21Å and $Al_2O_3$ has lattice constants a=4.76Å and c=12.991Å. In the growth process of ZnO buffer layer on $Al_2O_3$ substrate, the c-planes of ZnO rotates by $30^0$ in the basal c-plane of $Al_2O_3$ [14]. The hexagonally placed oxygen sites in $Al_2O_3$ (001) plane (figure 2a) have a lattice spacing of 2.75Å (i.e. $a_{Al2O3}/\sqrt{3}$) and the bulk lattice constant of ZnO is 3.24Å. This lattice mismatch between ZnO and hexagonally placed oxygen spacing (2.75Å) on $Al_2O_3$ creates an apparent stress in the ZnO lattice. Due to this stress, lattice constant of ZnO thin film deposited on $Al_2O_3$ decreases to 3.20Å. Now BZN ( with bulk lattice constant a=10.56Å) is deposited on to this stressed ZnO layer. The growth of systems with such a large lattice misfit is possible only with domain matching growth, where matching can be accommodated by matching planes of BZN and ZnO. The domain matching growth mechanism of BZN on ZnO can be described as follows. The $A_2B_2O_7$ pyrochlore structure can be described by the formula $B_2O_6.A_2O'$. This structure is built of two interpenetrating networks $BO_6$ octahedra-sharing vertices, form a three-dimensional network and resulting in large cavities which contain the O' and A atoms, which themselves forms a second cuprite-like $A_2O'$ tetrahedral net. The octahedral $B_2O_6$ network consists of {111} sheets of octahedra, sharing corners to form six- and three membered rings; these sheets are often referred to as ‘‘hexagonal tungsten bronze’’ (HTB) layers [21-23] as shown in figure 2b. The O' ions, located between the HTB layers in the large cavities, are surrounded by four A cations with the $A_4O'$ tetrahedral sharing corners. The preferential arrangement of BZN (222) on the ZnO buffer

layer occurs by the hexagonal arrangement of A-site atoms in BZN for the (111) plane of pyrochlore structure corresponding to the hexagonally placed oxygen sites of ZnO (0001) plane. Thus there is a domain matching of BZN ($2\bar{2}0$) plane with ZnO ($\bar{1}00$) plane across the film-buffer interface. In the case of BZN thin film grown directly on $Al_2O_3$ without ZnO buffer layer, the hexagonally placed A-site atoms in BZN orient themself directly on the oxygen sites of $Al_2O_3$ (0001) plane (figure 2). The spacing of oxygen sites in $Al_2O_3$ (figure 2a) is less than the A-site spacing of BZN. So there will be a stress in BZN lattice when it is directly grown on $Al_2O_3$, compared to the corresponding growth of BZN on ZnO buffer. This results in the polycrystalline growth of BZN thin film grown directly on $Al_2O_3$ substrate. When the first ZnO buffer layer is deposited on to $Al_2O_3$, ZnO lattice get stressed because of the lattice mismatch between ZnO and $Al_2O_3$. For the second ZnO buffer layer, the lattice for the same is relaxed on the first ZnO layer and stress decreases, which makes the second ZnO buffer layer, a domain matched layer for BZN.

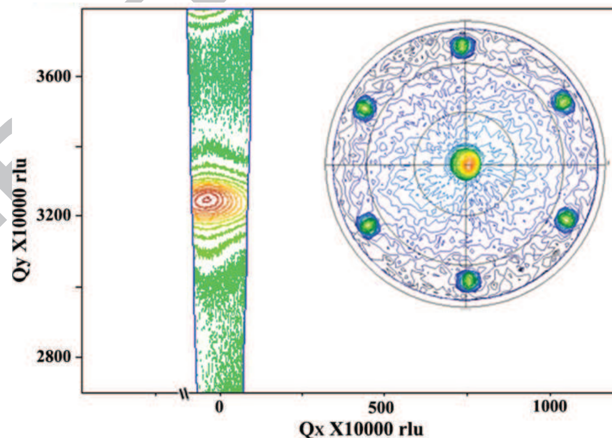


**Figure 3.** The reciprocal space mapping corresponding to BZN (222) plane. Inset shows the X-ray pole figure plot fixed at 2θ angle corresponding to BZN (222).

ACCEPTED MANUSCRIPT

Figure 3 shows the Reciprocal Space Mapping (RSM) measurements from the (222) reflection on same sample. RSM shows, not only this (222) peak located at the center of the RSM, but also another tail of reflection at the higher angle side of the RSM that is locating same direction with respect to reciprocal origin, which corresponds to BZN (444). The elongation of reciprocal space point of this peak is along with omega scan (horizontal direction), and small in omega-2theta direction (vertical). From this, we can conclude that the d-spacing distribution is small (uniform d-spacing over the sample), compared to angular distribution of this d-spacing. Inset of the figure 3 shows the pole figure analysis for the BZN thin film grown on double ZnO buffer. The pole figure plot corresponding to BZN (222) plane shows one strong spot at the centre ($\psi = 0^0$ and $\varphi = 0^0$) and a 6-fold reflection at $\psi = 70.5^0$ at every $60^0$ along the phi axis. Normally (222) oriented pyrochlore structures with Fd3m space symmetry will produce one pole at $\psi = 0^0$ and $\varphi = 0^0$ and three poles at $\psi = 70.5^0$ with an angular distance of $120^0$ in $\varphi$ [ $(22\bar{2}),(2\bar{2}2),(\bar{2}22)$ diffractions] in the pole figure plot [24]. However there are three additional poles displayed, which can give some additional structural information. By rotating the (222) oriented crystals by $60^0$ about the normal to the film surface, the three additional diffraction poles at $\psi = 70.5^0$ appears. They can be represented as $(\bar{2}\bar{2}2),(\bar{2}2\bar{2}),(2\bar{2}\bar{2})$. These diffraction poles occur due to twinning of the (222) oriented crystals by $60^0$. Figure 2c shows the prismatic environment of the A-cations in the pyrochlore structure. Here for the (222) plane, Zn ions can have two stacking sites, each separated by $60^0$ are possible as shown by the two black solid circles in figure 2. The intensities of all the six spots ($2\times 3$ reflections) are almost the same, which indicates that both orientations of the (222) planes (both in-plane and $60^0$ twinned) are equally probable. Also this $60^0$ twinning of the lattice sites results in the larger elongation of reciprocal space point along $\omega$-direction as depicted in RSM. Thus it confirms that BZN thin film

ACCEPTED MANUSCRIPT

ACCEPTED MANUSCRIPT

not only has an in-plane epitaxial orientation, but also has an out of plane epitaxial orientation. This demonstrates the first successful domain matching epitaxial growth of cubic BZN thin films.

Domain matching epitaxy (DME), where integral multiples of lattice planes are matched across the interface, provides a nice description of the interfacial structure of these systems. To verify this interfacial structure, we performed cross-sectional HRTEM measurements. Figure 4a is the HRTEM micrograph of the $Al_2O_3$-ZnO-BZN interface, which shows the epitaxial growth of BZN film with an atomically sharp interface demonstrating no intermediate reaction layer.

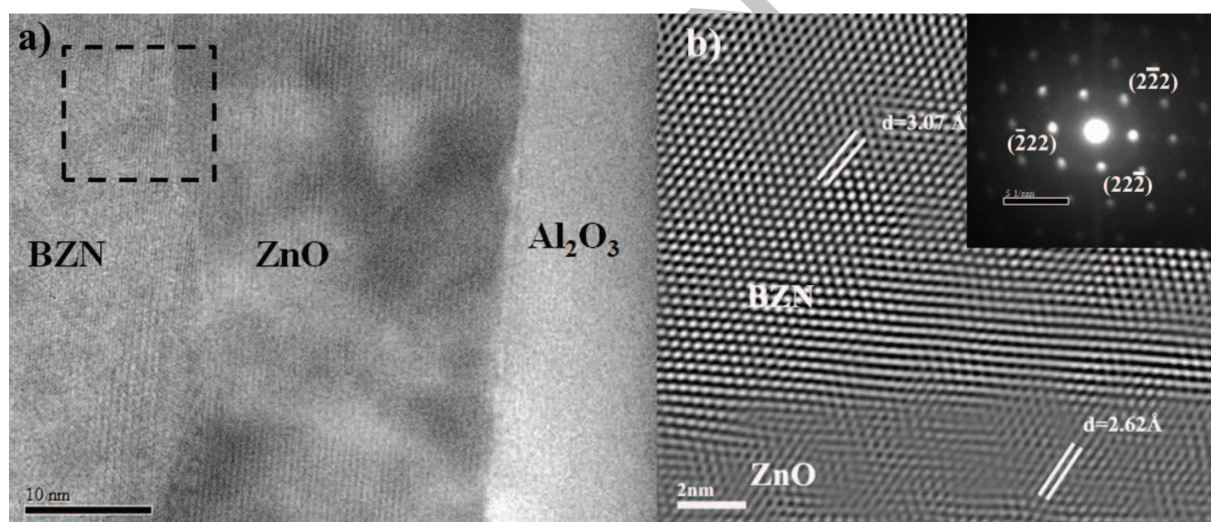


**Figure 4.** (a) HRTEM micrograph of BZN-ZnO-$Al_2O_3$ film cross section (b) Fourier transform of the HRTEM image of the black box area marked in figure (a) showing strong alignment of BZN (222) orientation with d-spacing of 0.307 nm. Inset shows the SAED pattern from BZN thin film.

The cross sectional HRTEM image shows a clear interface between BZN and ZnO thin film. The Fourier transform of the selected area in figure 4a is shown in figure 4b. It shows a well aligned BZN (222) orientation with d-spacing 3.07Å, which agrees well with that obtained

from XRD measurements and very close to the bulk value (3.05Å). The d-spacing for ZnO measured from HRTEM image is 2.62 Å which is close to that of the bulk value (2.64Å). The SAED pattern shows sharp intense spots from BZN (222) plane, which indicates the highly crystalline nature of BZN thin films. There are six intense spots around the central spot similar to that obtained in the pole figure analysis.

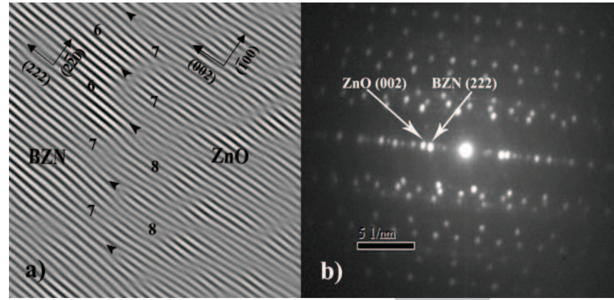


**Figure 5.** a) Domain epitaxy in the BZN/ZnO system, Fourier-filtered image of matching of BZN $(2\bar{2}0)$ and ZnO $(\bar{1}00)$planes for 6/7 and 7/8 domains in high-resolution cross section b) corresponding electron diffraction pattern showing the alignment of planes in BZN and ZnO.

Domain epitaxial growth of BZN $(2\bar{2}0)$ with cubic pyrochlore structure on ZnO $(\bar{1}00)$ substrate occurs via matching of 7 or 8 ZnO $(\bar{1}00)$ planes with 6 or 7 BZN $(2\bar{2}0)$ planes. The spacing of BZN $(2\bar{2}0)$ planes (*3.77Å*) is close to 17.8% residual mismatch with $(\bar{1}00)$ planes of ZnO (3.20Å). Taking the 6×d{BZN$(2\bar{2}0)$} and 7×d{ZnO$(\bar{1}00)$} domain matching structure, we have a residual mismatch defined by

$$m = \left(6\times a_e / 2\sqrt{2} - 7\times a_b\right)/\left(7\times a_b\right) = 0.0098$$

and for 7×d{BZN$(2\bar{2}0)$} and 8×d{ZnO$(\bar{1}00)$}, the residual strain is

$$m = \left(7\times a_e / 2\sqrt{2} - 8\times a_b\right)/\left(8\times a_b\right) = 0.03$$



ACCEPTED MANUSCRIPT

ACCEPTED MANUSCRIPT

Where, $a_e$ and $a_b$ are respectively the lattice constants of the epilayer BZN and buffer layer ZnO. Thus the 6/7 domain matching structure effectively accommodates the 17.8% mismatch by the introduction of periodic dislocations localized at the interface leaving a residual 0.98% tensile strain in the BZN films. This quasi-periodic dislocations can be clearly seen in the Fourier-filtered image of the BZN film-ZnO buffer interface, with every 6 or 7 planes of BZN $(2\bar{2}0)$ matching with 7 or 8 planes of ZnO $(\bar{1}00)$ as shown in figure 5a. This gives clear confirmation of the DME of BZN thin films on ZnO buffer layer. Figure 5b shows the SAED pattern of the BZN-ZnO interface, where the alignment of BZN (222) planes with ZnO (002) planes is clearly shown.

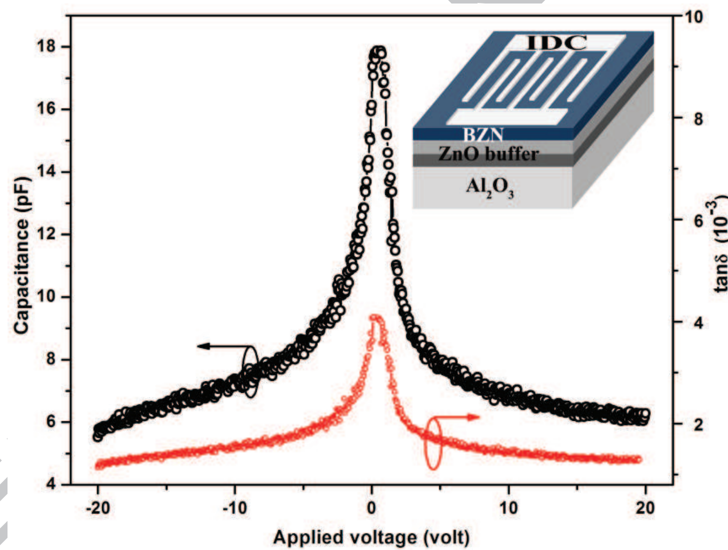


**Figure 6.** The bias voltage dependence of capacitance and dissipation factor for the fabricated Inter Digital Capacitor (IDC) over epitaxial BZN thin film. Inset shows schematic representation of the IDC structure patterned over the BZN thin film.

Electrical characterization of the epitaxially grown BZN thin film was carried out by patterning inter digital capacitors (IDC) on the surface of BZN thin film using a standard

ACCEPTED MANUSCRIPT

photolithographic process. The patterned IDC have a total of seven fingers with a finger width of 0.5 mm and a gap of 0.5 mm as shown in the inset of figure 6. Capacitance-Voltage measurements (Figure 6 ) were performed at 1 MHz and the voltage applied was swept from -20 to +20 V. The epitaxial BZN thin film on $Al_2O_3$ with ZnO buffer layer exhibits a maximum capacitance of 18 pF around zero bias and a minimum of 5.6 pF at 20 volt, that gives a high dielectric tunability of 68% at an applied voltage 20 volts, with the expression $T=[C_{max}-C_{min}/C_{max}]\%$. There is a very slight asymmetry in the C-V curve, it may be due to the contribution from the semiconducting ZnO buffer layer. Dissipation factor (tanδ) was also measured as a function of bias voltage. The measured dissipation factor, was of the order of $10^{-3}$ in the MHz range. The observed maximum dissipation factor occurs at zero electric field as expected since it is a measure of the free charge carriers responding to high frequency signal. The results indicate that the epitaxial growth of BZN thin film on $Al_2O_3$ contributed to the enhancement in dielectric tunability [25-27] while keeping the dielectric loss low.

## 4. Conclusion

Epitaxial growth of $Bi_{1.5}Zn_1Nb_{1.5}O_7$ (222) thin films has been achieved with a ZnO double buffer layer on $Al_2O_3$ substrate by pulsed laser deposition. BZN thin films deposited directly onto $Al_2O_3$ were polycrystalline in nature. The double ZnO buffer layer effectively reduced the lattice mismatch and favored the domain matching epitaxial growth of BZN thin film on ZnO buffer layer. The pole figure analysis and reciprocal space mapping revealed the single crystalline nature of the thin film. The two pairs of three highly intense poles at $\psi=70.5^0$ with an angular distance of $\varphi=60^0$ indicates both in-plane and out of plane epitaxial growth of BZN (222) plane. Similar intensity of all poles indicates that both in-plane and $60^0$ twinned orientation are equally probable. The cross sectional HRTEM image shows a clear interface between BZN and

ACCEPTED MANUSCRIPT

ACCEPTED MANUSCRIPT

ZnO thin film. The sharp intense spots in the SAED pattern also indicate the crystalline nature of BZN thin film. The Fourier filtered images shows that there is a perfect domain matching of 6-BZN $(2\bar{2}0)$ planes corresponding to 7-ZnO $(\bar{1}00)$ planes, which results in less than 1% residual strain. This clearly reveals the domain matching epitaxial growth of BZN on ZnO buffer layer. The fabricated capacitor on the epitaxial film showed significantly higher tunability while keeping low dielectric loss. The growth approach based on the double ZnO buffer layer gives a convenient way to fabricate high quality epitaxial ferroelectric films on $Al_2O_3$.

**Acknowledgements**

The authors would like to thank Department of Science and Technology for the financial support, Indo-Spanish joint programme of co-operation in science and technology for HRTEM measurements and Indian Nano Users Program (INUP) for providing the lithography facility.

**References**

[1] T. Yamada, K. F. Astafiev, V. O. Sherman, A. K. Tagantsev, P. Muralt, and N. Setter, Appl. Phys. Lett. **86**, 142904 (2005).

[2] A. K. Tagantsev, V. O. Sherman, K. F. Astafiev, J. Venkatesh, and N.Setter, J. Electroceram. **11**, 5 (2003).

[3] A. Perrin, A. Rousseau, D. Fasquelle, V. Laur, V. Bouquet, S. Deputier, P. Laurent, G. Tanne, F. Huret, J. C. Carru and M. Guilloux-Viry, Phase Transitions, **81**, Nos. 7–8, 643, (2008).

ACCEPTED MANUSCRIPT

ACCEPTED MANUSCRIPT

[4] Q. Simon, Y. Corredores, X. Castel, R. Benzerga, R. Sauleau, K. Mahdjoubi, A. L. Febvrier, S. Députier, M. Guilloux-Viry, L. Zhang, P. Laurent, and G. Tanné, Appl. Phys. Lett. **99**, 092904 (2011).

[5] J. H. Haeni, P. Irvin, W. Chang, R. Uecker, P. Reiche, Y. L. Li, S. Choudhury, W. Tian, M. E. Hawley, B. Craigo, A. K. Tagantsev, X. Q. Pan, S. K. Streiffer, L. Q. Chen, S. W. Kirchoefer, J. Levy, and D. G. Schlom, Nature London **430**, 758 (2004).

[6] N. A. Pertsev, A. K. Tagantsev, and N. Setter, Phys. Rev. B **61**, R825 (2000).

[7] Y. Fujisaki, K. Iseki and H. Ishiwara, Mater. Res. Soc. Symp. Proc. **786**, 297 (2003).

[8] D. Y. Chen, T. E. Murphy and J. D. Phillips, Thin Solid Films **491,** 301 (2005).

[9] N. Ashkenov, M. Schubert, E. Twerdowski, T. Wenckstern, B. N. Mbenkum, H. Hochmuth, M. Lorenz, W. Grill, and M. Grundmann, Thin Solid Films **486**, 153 (2005).

[10] J. T. Evans, R. I. Suizu and L. L. Boyer, Appl. Surf. Sci. **117/118**, 413 (1997).

[11] V. P. Afanas'ev, D. Y. Bulat, E. Y. Kaptelov and I. P. Pronin, Technol. Phys. Lett. **30**, 518 (2004).

[12] K. H. Cho, M. G. Kang, S. M. Oh , C. Y. Kang, Y. P. Lee, and S. J. Yoon, Thin Solid Films, **518**, 6277 (2010).

[13] J. Wu and J. Wang, J. Appl. Phys. **108**, 034102 (2010).

[14] J. Narayan, B. C. Larson, J. Appl. Phys. **93**, 278 (2003).

[15] L. M. B. Alldredge, W. Chang, S. B. Qadri, S. W. Kirchoefer, and J. M. Pond, Appl. Phys. Lett. **90**, 212901 (2007).

[16] X. Zhu, J. Zhu, S. Zhou, Z. Liu, N. Ming, H. L. Chan, C. L. Choy, and K. Wong, J. Mater. Res. **23**, 3 (2008).

ACCEPTED MANUSCRIPT

ACCEPTED MANUSCRIPT

[17] L. Z. Cao, W. Y. Fu, S. F. Wang, Q. Wang, Z. H. Sun, H. Yang, B. L. Cheng, H. Wang and Y. L. Zhou, J. Phys. D: Appl. Phys. **40**, 1460 (2007).

[18] B. Xiao, V. Avrutin, H. R. Liu, E. Rowe, J. Leach, X. Gu, U. Ozgur, and H. Morkoç, Appl. Phys. Lett. **95**, 010927 (2009).

[19] T. Yamada, P. Muralt, V. O. Sherman, C. S. Sandu, and N. Setter, Appl. Phys. Lett. **90**, 142911 (2007).

[20] P. S. Krishnaprasad, M. Sebastian, F. Rojas, A. Antony and M. K. Jayaraj, Mater. Res. Soc. Symp. Proc. **1454** (2012).

[21] Y. Liu, R. L. Withers, T.R. Welberry, H. Wang, H. Du, J. Solid State Chem. **179**, 2141 (2006).

[22] I. Levin, T. G. Amos, J. C. Nino, T. A. Vanderah, C. A. Randall and M. T. Lanagan, J. Solid State Chem. **168**, 69 (2002).

[23] T. J. White, Am. Miner. **69**, 1156 (1984).

[24] P. F. Fewster, X ray scattering from semiconductors (2nd Edition), (Imperial College Press, 2003), p.292.

[25] L. Z. Cao, W. Y. Fu, S. F. Wang, Q. Wang, Z. H. Sun, H. Yang, B. L. Cheng, H. Wang and Y. L. Zhou, J. Phys. D: Appl. Phys. **40**, 2906 (2007).

[26] J. Lu and S. Stemmer, Appl. Phys. Lett. **83**, 2411 (2003).

[27] W. Ren, S. Trolier-McKinstry,C. A. Randall, and T. R. Shrout, *J. Appl. Phys.* **89**, 767 (2001).

ACCEPTED MANUSCRIPT

ACCEPTED MANUSCRIPT

**Figure captions:**

**Figure 1.** a) The JCPDS data of BZN and the XRD ω-2θ scan of the BZN film deposited b) directly on to $Al_2O_3$ substrate c) with single ZnO buffer layer and d) with double ZnO buffer layer.

**Figure 2.** a) Schematic of arrangement of atoms in the basal plane of ZnO and $Al_2O_3$ b) $B_2O_6$ networks in the $A_2B_2O_7$ pyrochlore forming a hexagonal tungsten bronze structure c) The essentially hexagonal prismatic environment of the A cations in the $A_2B_2O_7$ pyrochlore structure type of BZN projected along [111].

**Figure 3.** The reciprocal space mapping corresponding to BZN (222) plane. Inset shows the X-ray pole figure plot fixed at 2θ angle corresponding to BZN (222).

**Figure 4.** (a) HRTEM micrograph of BZN-ZnO-$Al_2O_3$ film cross section (b) Fourier transform of the HRTEM image of the black box area marked in figure (a) showing strong alignment of BZN (222) orientation with d-spacing of 0.307 nm. Inset shows the SAED pattern from BZN thin film.

**Figure 5.** a) Domain epitaxy in the BZN/ZnO system, Fourier-filtered image of matching of BZN $(2\bar{2}0)$ and ZnO $(\bar{1}00)$planes for 6/7 and 7/8 domains in high-resolution cross section b) corresponding electron diffraction pattern showing the alignment of planes in BZN and ZnO.

ACCEPTED MANUSCRIPT

ACCEPTED MANUSCRIPT

**Figure 6.** The bias voltage dependence of capacitance and dissipation factor for the fabricated IDC over epitaxial BZN thin film. Inset shows schematic representation of Inter Digital Capacitor (IDC) structure patterned over the BZN thin film.

ACCEPTED MANUSCRIPT

ACCEPTED MANUSCRIPT

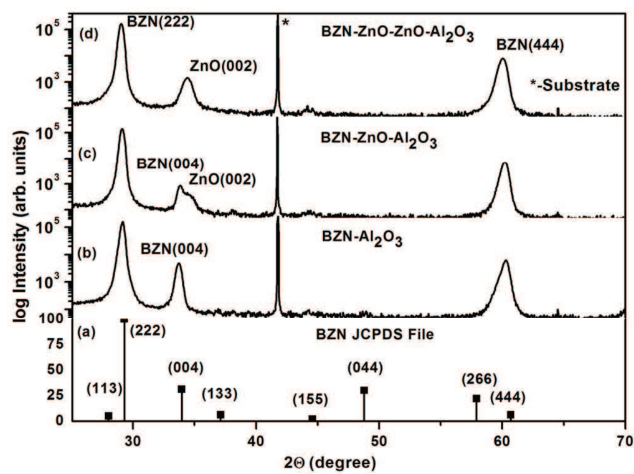


ACCEPTED MANUSCRIPT

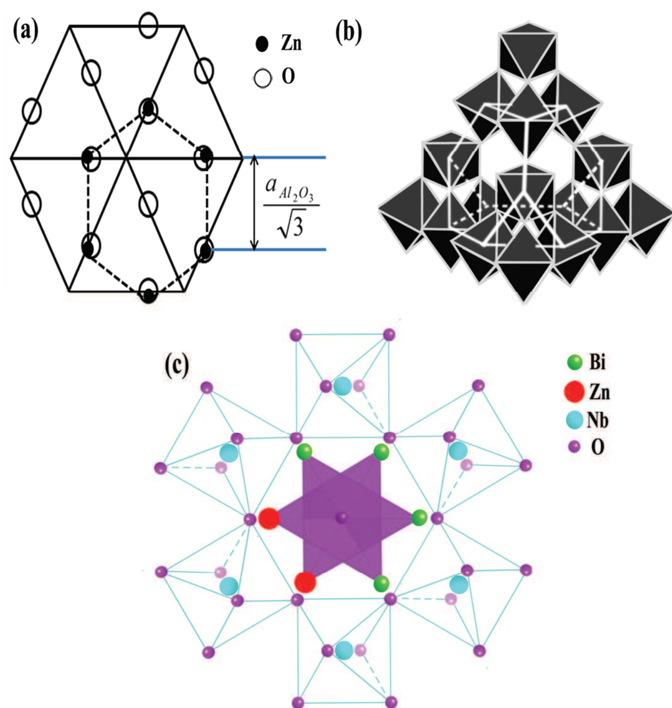


ACCEPTED MANUSCRIPT

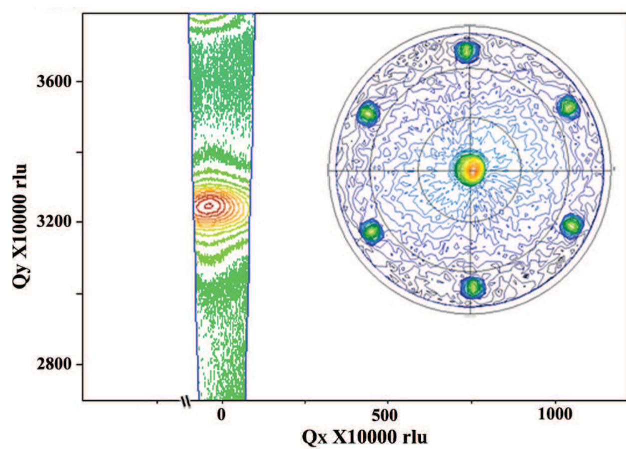


ACCEPTED MANUSCRIPT

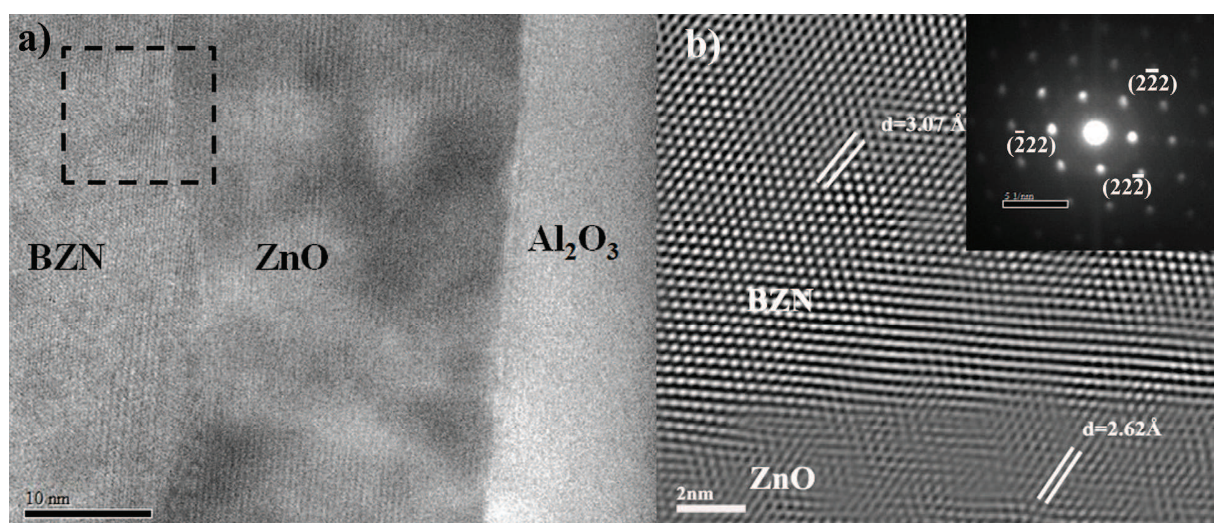


ACCEPTED MANUSCRIPT

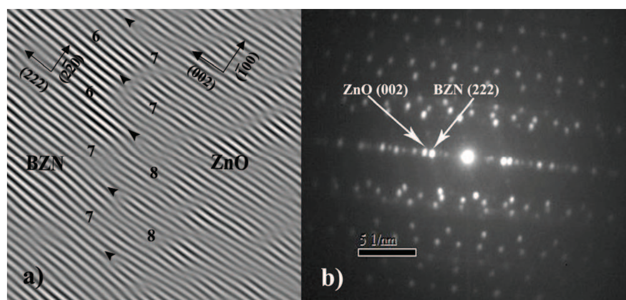


ACCEPTED MANUSCRIPT

ACCEPTED MANUSCRIPT

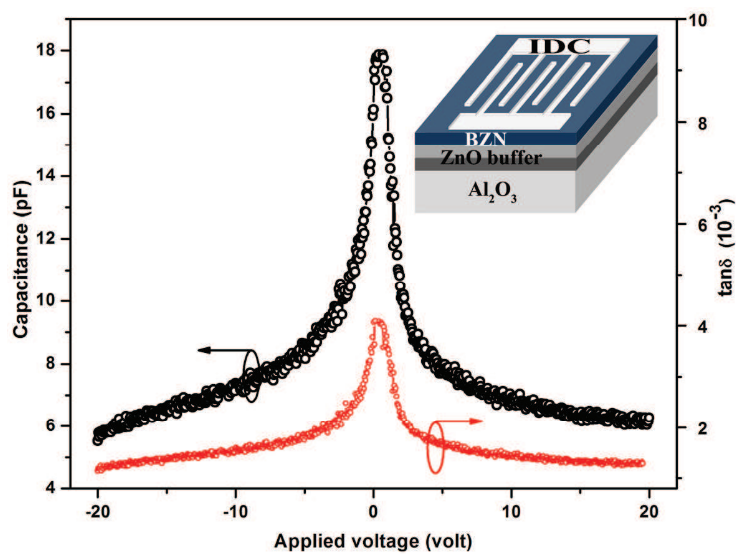


ACCEPTED MANUSCRIPT